

Natural Intrauterine Infection with Schmallenberg Virus in Malformed Newborn Calves

Calixte Bayrou,¹ Mutien-Marie Garigliany,¹
Michael Sarlet, Arnaud Sartelet,
Dominique Cassart, and Daniel Desmecht

We surveyed morphologic alterations in calves in Belgium that were naturally infected in utero by Schmallenberg virus (SBV) and born with deformities during January–March 2012. SBV-specific RNA was distributed unevenly in different tissues. Natural intrauterine SBV infection of calves might cause serious damage to the central nervous system and muscles.

During summer and fall 2011, a nonspecific febrile syndrome characterized by hyperthermia and decreased milk production was reported in adult dairy cows from farms in the Netherlands and Germany (1,2). In November 2011, an enzootic outbreak of abortions, stillbirths, and term births of lambs, kids, and calves that exhibited neurologic signs and/or musculoskeletal malformations emerged throughout northwestern Europe (3,4). Both syndromes were associated with the presence in the blood (adults) or in the central nervous system (CNS) (newborns) of the genome of a new orthobunyavirus, which was named Schmallenberg virus (SBV) after the place where the first positive samples were collected (3,4). SBV belongs to the Simbu serogroup (5) and, like its phylogenetic relatives Akabane and Aino viruses, can cross the placenta (6). Because this new viral disease of ruminants emerged 3 years ago, information is limited. We comprehensively surveyed morphologic alterations in calves naturally infected in utero. In addition, we report the distribution of SBV-specific RNA in the different tissues of these calves, which has implications for diagnosis.

The Study

In Belgium each year during January–June, field veterinarians refer ≈30 newborn calves per month for necropsy to the University of Liège Faculty of Veterinary Medicine

(Liège, Belgium). During January–March 2012, the consequences of SBV infection on bovine fetuses were not yet known, which prompted the staff to look systematically for the new virus in all deformed calves and in calves that died spontaneously without obvious cause. Among the 67 animals in these categories, SBV genetic material was detected in 15 calves by reverse transcription quantitative PCR, and IgG specific for SBV nucleoprotein was systematically highlighted in their serum by ELISA. In addition, all attempts to retrieve the genetic material of bluetongue virus 8 and bovine viral diarrhea virus from the tissues of these 15 seropositive calves failed. None of these calves carried the mutation responsible for noninfectious arthrogryposis in local livestock. These 15 calves, in which both SBV RNA and antibodies against SBV were detected, are the subject of this study.

Detailed information about the methods used to examine the calves is available in online Technical Appendix 1 (<http://wwwnc.cdc.gov/EID/article/20/8/12-1890-Techapp1.pdf>). A detailed description of the lesions found in SBV-infected calves is provided in online Technical Appendix 2 (<http://wwwnc.cdc.gov/EID/article/20/8/12-1890-Techapp2.pdf>).

SBV-positive animals weighed significantly less than expected (32 kg ± 15 kg vs. 49 kg ± 4 kg, $p < 0.05$). The body mass deficit, severity of deformities in whole-body conformation, and amount of skeletal muscle were obviously correlated (Table 1; online Technical Appendix 3 Figure 1, <http://wwwnc.cdc.gov/EID/article/20/8/12-1890-Techapp3.pdf>).

We observed overall permanent deviations of the axial skeleton in all 3 planes (online Technical Appendix 3 Figure 2), the most common being a lateral deviation of the cervical spine (torticollis). In the most distorted animals, the torticollis was accompanied by a dorso-ventral deviation of the thoracolumbar spine. Most SBV-infected calves displayed joint fixation of 1 or all joints of ≥1 limbs (arthrogryposis). Tendons spanning fixed joints were shorter than expected, and corresponding muscles displayed decreased mass and altered color. Often the animal's head was distorted, having a horse-like or pig-like shape, brachygnathism, prognathism, and/or diverging sagittal axes (online Technical Appendix 3 Figure 3).

We systematically observed major alterations after we opened the skull and spinal canal (Figure 1; online Technical Appendix 3 Figure 4). These changes involved the spinal cord and the telencephalon, whereas the brainstem and cerebellum were kept intact (although 1 cerebellum was hypoplastic). We consistently observed a decrease in the cross-sectional area of the spinal cord (Figure 2), which correlated positively with the magnitude of axial/appendicular musculoskeletal deformities (online Technical Appendix

Author affiliation: University of Liège, Liège, Belgium

DOI: <http://dx.doi.org/10.3201/eid2008.121890>

¹These authors contributed equally to this article.

Table 1. Macroscopic characteristics of 15 SBV-infected newborn calves at necropsy, Belgium, January–March 2012*

Characteristic	WBD-0†	WBD-1†	WBD-2†	WBD-3†	Total no. calves
No. calves	2	4	4	5	15
Method of death					
Euthanasia	2	3	0	0	5
Spontaneous	0	1	4	5	10
Bodyweight, kg‡§	49 ± 4	39 ± 3	34 ± 3	21 ± 2	
Axial musculoskeletal system					
Defect location					
Cervical	0	2	4	5	11
Thoracic	0	0	2	5	7
Lumbar	0	0	0	5	5
Type of deviation					
Lateral	0	2	4	5	11
Dorso-ventral	0	0	1	4	5
Helicoidal	0	0	1	4	5
Appendicular musculo-skeletal system					
Arthrogryposis (≥1 limb involved)	0	3	4	5	12
Symetric limb involvement	NA	3	3	5	11
Forelimb/hind limb involvement	NA	0	1	5	6
Forelimbs only	NA	2	3	0	5
Hind limbs only	NA	1	0	0	1
Head					
Coaptation defect					
Prognathism	0	0	0	1	1
Brachygnathism	0	1	1	2	4
Altered profile					
Horse-like	0	1	1	0	2
Pig-like	0	0	0	2	2
Broken sagittal axis	0	1	2	2	5
Central nervous system					
Porencephaly	2	3	3	1	9
Hydranencephaly	1	1	0	1	3
Hydrocephaly	0	0	1	4	5
Cerebellar hypoplasia	0	0	0	1	1
Micromyelia	2	4	4	5	15

*Fifteen newborn calves infected in utero by SBV were categorized according to the extent of their deformities. The table lists the gross morphologic changes observed at necropsy. SBV, Schmallenberg virus; WBD, whole-body deformity score; NA, not applicable.

†Animals with neurologic signs and apparently normal body shape were given a WBD of 0; those with altered body shape were scored 1, 2, or 3 depending on whether 1, 2, or 3 skeletal segments were deformed, respectively (spine, forelimbs, or hind limbs). All values are number of calves unless otherwise indicated.

‡Mean ± SD.

§Bodyweight of age-matched Belgian Blue healthy calves is 49.2 kg ± 7.1 kg (7).

3 Figure 5). The neopallial part of the telencephalon was always decreased, giving 3 distinct morphotypes. In some calves, we detected multiple, bilateral, and randomly located cystic cavities, most of which communicated with the ipsilateral ventricle (porencephaly). In other cases, all that remained from the neopallium was a thin, nearly transparent membrane, sometimes with a few floating smooth-surfaced islets resembling cortex (hydranencephaly). Finally, in a third subset of calves, the brain appeared normal, but we observed a severe, bilateral, and symmetric dilatation of lateral ventricles after section (hydrocephaly).

Microscopic examination of the spinal cord revealed a significant decrease in neuron numbers, the magnitude of which correlated positively with the severity of whole-body deformities (Table 2). Muscle sections displayed a diffuse pattern of increased fiber size variation with connective tissue and adipocyte infiltrations (online Technical Appendix 4 Table 1, <http://wwwnc.cdc.gov/EID/article/20/8/12-1890-Techapp4.pdf>).

The viral RNA was always present in the CNS and sometimes in the lungs and colon (online Technical Appendix 4 Table 2). When the entire cohort was considered, SBV was detected in all parts of the CNS. When we examined the animals individually, however, the detection rate varied depending on the segment (online Technical Appendix 4 Table 2). The virus was almost always detected in the spinal cord (93%) and the neopallium (87%); often in the midbrain (83%) and pons (67%); and about half the time in the diencephalon, cerebellum, and paleopallium. The practical implications of these findings for routine diagnosis are highlighted separately (online Technical Appendix 5, <http://wwwnc.cdc.gov/EID/article/20/8/12-1890-Techapp5.pdf>).

Conclusions

Our findings show that natural in utero infection of the bovine fetus by SBV may result in serious damage to the CNS and muscles. Mechanistic hypotheses that could

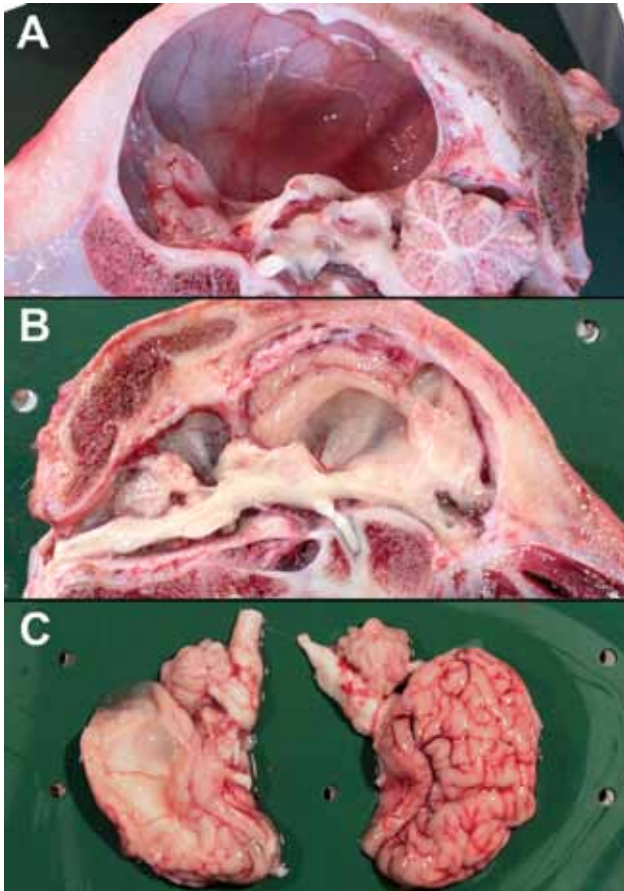


Figure 1. Deformities of the brain in calves naturally infected in utero with Schmallenberg virus, Belgium, January–March 2012. A) Hydranencephaly. B) Hydrocephaly and cerebellar hypoplasia. C) Porencephaly.

explain these alterations are discussed in online Technical Appendix 6 (<http://wwwnc.cdc.gov/EID/article/20/8/12-1890-Techapp6.pdf>). Similar to the situation with Akabane virus infection (8), the clinical picture shown by in utero SBV-infected newborn calves is likely to depend largely on the age of the fetus at the time of infection. The infection must be quickly contained if the fetus is infected when immunocompetent (≥ 120 –150 days after conception), and we deduce that damages inflicted by the virus consequently have no or little effect on its further development. Conversely, the infection probably spreads more easily and lasts much longer if the virus contaminates an immunologically immature fetus. Because transplacental infection is possible only when the first placentome is present (30 days after conception in cattle), the window during which the infection of a bovine fetus might lead to a porencephaly/hydranencephaly-micromyelia-arthrogryposis syndrome ranges from 30 to 150 days after conception. The degree of overall body deformity correlated with a progressively greater reduction in the size of the

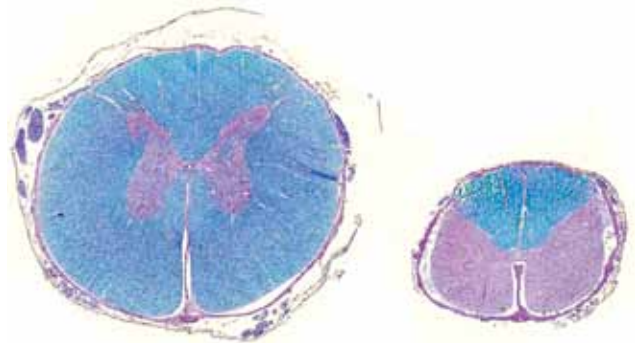


Figure 2. Micromyelia. Age- and site-matched spinal cord transversal histologic section at the level of C4. Left, control calf; right, Schmallenberg virus (SBV)-infected calf. Note atrophy/hypoplasia and prominent deficiency of stainable myelin in ventral and lateral tracts of SBV-infected calf. Luxol fast blue staining.

spinal cord (as determined by spinal cord:foramen magnum ratio) and with fewer spinal neurons, suggesting that the lack of movement leading to arthrogryposis results directly from the spinal cord lesions, leading to denervation atrophy of skeletal muscle. This primary role for the spinal cord lesion is further supported by the tendency of forelimbs and hind limbs to be affected bilaterally because muscle involvement might be expected to lead to more randomly distributed lesions.

When SBV virus infects the bovine fetus during the risk window mentioned above and causes neuromuscular defects, its genetic material remains detectable at term—thus 4 months later—at a minimum. The physical form of this persisting virus and the way it persists in the face of the seroconversion are unknown. The hypothesis of the existence of sites of persistence must be addressed, for example, in the CNS ($\approx 90\%$ of cases were virus positive at term) or lungs ($\approx 30\%$). In practice, a priority is to establish whether SBV persists in calves infected in utero but born asymptomatic.

Acknowledgments

We thank Martin Beer and Bernd Hoffmann for kindly providing help for the setup and validation of the reverse transcription quantitative PCR procedure and for confirming a set of results. We also are grateful to Deborah Kleijnen and Pauline Meirlaen for their skilled technical support through the study.

The study was supported by a grant from the Research Council in Life Sciences of University of Liège.

References

- Hoffmann B, Scheuch M, Höper D, Jungblut R, Holsteg M, Schirmeier H, et al. Novel orthobunyavirus in cattle, Europe, 2011. *Emerg Infect Dis.* 2012;18:469–72. <http://dx.doi.org/10.3201/eid1803.111905>

Table 2. Correlation between spinal neuron counts and axial muscle histologic changes in 15 SBV-infected newborn calves, Belgium, January–March 2012*

Structure examined	Control calves	WBD/calf ID														
		WBD-0		WBD-1				WBD-2				WBD-3				
		A	B	C	D	E	F	G	H	I	J	K	L	M	N	O
Axial muscles, histology																
Musculus semispinalis capitis, cas	0	NT	0	0	0	3	0	3	3	NT	3	3	3	3	3	3
Musculus semispinalis capitis, ces	0	NT	1	0	0	2	0	3	3	NT	3	3	3	3	3	3
Spinal cord																
Dorsal horn neurons, no.																
Left dorsal horn	12 ± 5	NT	11	21	4	5	10	5	1	NT	4	0	0	0	7	3
Right dorsal horn	11 ± 4	NT	23	17	6	5	10	7	3	NT	5	1	0	0	5	0
Ventral horn neurons, no.																
Left ventral horn	50 ± 10	NT	56	57	15	1	45	9	1	NT	0	0	0	0	7	0
Right ventral horn	50 ± 4	NT	47	55	14	3	31	7	0	NT	0	0	0	0	4	0

*Extent of histologic changes was reported semiquantitatively by using a score of 0, 1, 2, or 3 depending on whether the histologically normal tissue extended over 100%, 75%–100%, 25%–75%, or <25% of the area examined and intensity of shading reflects these values. Neurons were enumerated in transverse sections of the spinal cord corresponding to C4. Intensity of shading reflects the magnitude of neuron deficits. SBV, Schmallenberg virus; WBD, whole-body deformity score; NT, not tested; cas, concave side; ces, convex side.

- Muskens J, Smolenaars AJ, van der Poel WH, Mars MH, van Wuijckhuise L, Holzhauser M, et al. Diarrhea and loss of production on Dutch dairy farms caused by the Schmallenberg virus [in Dutch]. *Tijdschr Diergeneeskd.* 2012;137:112–5.
- Garigliany M-M, Hoffmann B, Dive M, Sartelet A, Bayrou C, Cassart C, et al. Schmallenberg virus in calf born at term with porencephaly, Belgium. *Emerg Infect Dis.* 2012;18:1005–6.
- van den Brom R, Lutikholt SJ, Lievaart-Peterson K, Peperkamp NH, Mars MH, van der Poel WH, et al. Epizootic of ovine congenital malformations associated with Schmallenberg virus infection. *Tijdschr Diergeneeskd.* 2012;137:106–11.
- Goller KV, Höper D, Schirmeier H, Mettenleiter TC, Beer M. Schmallenberg virus as possible ancestor of Shamonda virus. *Emerg Infect Dis.* 2012;18:1644–6. <http://dx.doi.org/10.3201/eid1810.120835>
- Garigliany MM, Bayrou C, Kleijnen D, Cassart D, Desmecht D. Schmallenberg virus in domestic cattle, Belgium, 2012. *Emerg Infect Dis.* 2012;18:1512–4. <http://dx.doi.org/10.3201/eid1809.120716>
- Kolkman I, Opsomer G, Aerts S, Hoflack G, Laevens H, Lips D. Analysis of body measurements of newborn purebred Belgian Blue calves. *Animal.* 2010;4:661–71. <http://dx.doi.org/10.1017/S1751731109991558>
- Charles JA. Akabane virus. *Vet Clin North Am Food Anim Pract.* 1994;10:525–46.

Address for correspondence: Daniel Desmecht, Department of Pathology, Faculty of Veterinary Medicine, University of Liège, B-4000 Liège, Belgium; email: daniel.desmecht@ulg.ac.be

Get the content you want delivered to your inbox.



Table of Contents
Podcasts
Ahead of Print Articles
CME
Specialized Content

Online subscription: wwwnc.cdc.gov/eid/subscribe.htm

Natural Intrauterine Infection with Schmallenberg Virus in Malformed Newborn Calves

Technical Appendix 1

Materials and Methods

Context

Field veterinarians refer \approx 2 200 dead animals per year for necropsy to the University of Liège Faculty of Veterinary Medicine. For cattle, a dedicated shuttle runs daily throughout Wallonia (Belgium) to remove and transport the bodies from the farms to the Faculty, which enables necropsy within a reasonable time, 12–48 hours after death in 90% of cases. During an \approx 6-month period beginning in January 2012, an unusual musculoskeletal syndrome event was recognized among referred newborn calves. The affected animals were born at term, without dystocia, and none of them had suckled or received colostrum. They displayed mild to severe deformities of axial and appendicular systems, and corresponding anamnestic data consistently mentioned severe antemortem behavioral and motor dysfunctions. The frequency of such cases was \approx 20 times that expected based on the 1980–2010 period.

Gross Pathology

The animals were examined by pathologists according to a standardized protocol. They were first weighed, and the average weight of the different cohorts defined hereafter was compared by using the Mann-Whitney test. To better reflect the diversity of clinical presentations, these calves were divided into 4 categories according to the severity of their musculoskeletal deformities (Technical Appendix 3, Figure 1, <http://wwwnc.cdc.gov/EID/article/20/8/12-1890-Techapp3.pdf>). Animals with neurologic signs and apparently normal body shape were given a whole-body deformity (WBD) score of 0. Those with altered body shape were scored 1, 2, or 3 depending on whether 1, 2 or 3 skeletal segments were deformed, respectively (spine, forelimbs, or hind limbs). In addition, the maximum widths of the foramen magnum and of the spinal cord at that level were measured. The occipital ratio reported is the result of dividing the second width by the first. After a thorough examination, the following organs

were sampled: brain, spinal cord, lung, myocardium, thymus, liver, spleen, kidney, duodenum, jejunum, ileum, colon, and skeletal muscles. From the brain, specimens from 6 distinct regions were sampled: olfactory bulb (paleopallium), cortex (neopallium), diencephalon, midbrain (mesencephalon), cerebellum, and pons (metencephalon). The spinal cord samples consisted of the segment corresponding to the fourth cervical vertebra. Nine skeletal muscles were sampled, 2 spinal muscles (semispinalis capitis and longissimus thoracis), 3 forelimb muscles (supraspinatus, extensor carpi radialis, and flexor carpi ulnaris), and 3 hind limb muscles (semimembranosus, quadriceps femoris, and peroneus tertius). For the semispinalis capitis, a piece of muscle was taken directly below the fourth cervical vertebra from either side of the pathologic curvature of the spine. Each tissue sample was then divided in 2 fragments: 1 was frozen at -80°C (for subsequent RNA extraction), and the other was immersed in 10% buffered formalin (histopathology). Postmortem serum was extracted from the cardiac ventricles and kept frozen at -20°C until use.

Histology

All tissues were routinely processed in paraffin wax, cut at 4- μm thickness, mounted on glass slides, deparaffinized in xylene, dehydrated in ethanol, and stained with hematoxylin and eosin. Luxol fast blue staining was chosen for visualizing myelin in spinal cord and efferent axons in ventral roots. Perls' acid ferrocyanide reaction was used to reveal iron compounds in the ferric state, with nuclear fast red for counterstaining. The control cohort included five 1-day-old calves that were simultaneously negative for viral RNA and Schmallenberg virus (SBV) IgG. The extent of histologic changes was reported semiquantitatively by using a score of 0, 1, 2, or 3 depending on whether the histologically normal tissue was 100%, 75%–100%, 25%–75%, or <25% of the area examined.

Detection of SBV-specific Antibodies

IgG against the nucleoprotein of SBV was detected in postmortem serum by using the ELISA kit (ID Screen Schmallenberg virus Indirect v.1) recently made available by ID.vet Innovative Diagnostics (ID.vet Innovative Diagnostics, Montpellier, France). In this assay, results are expressed as percentages of the reference signal yielded by a positive control serum, with serologic status defined by the manufacturer as negative ($\leq 60\%$), doubtful ($>60\%$ and $\leq 70\%$) or positive ($>70\%$). Positive and negative reference bovine serum was drawn within a previously archived bank (1).

Detection of Viral RNA

The virus genome was sought in the tissues of all animals belonging to ≥ 1 of the following categories: 1) calves with reported neurologic signs before death, 2) calves displaying musculoskeletal deformities, and 3) calves that died spontaneously soon after birth and in which no unequivocal cause of death was identified at necropsy. Tissue samples collected in the necropsy room were homogenized (Qiagen TissueLyser, Venlo, the Netherlands, 30 Hz for 2 min) in TRIzol reagent (Invitrogen, Merelbeke, Belgium), and total RNA was extracted from the resulting homogenate according to the manufacturer's instructions. Precipitated RNA was resuspended in 10% dimethyl sulfoxide (Sigma-Aldrich, Diegem, Belgium) and stored at -80°C until use. A Mastercycler pro thermocycler (Eppendorf, Rotselaar, Belgium) and a StepOnePlus real-time PCR system (Applied Biosystems, Gent, Belgium) were used for reverse transcription (RT) and quantitative PCR (qPCR), respectively. Detection of the SBV genome was performed according to Bilk et al. (2) and that of the bovine viral diarrhea virus (BVDV) genome according to La Rocca and Sandvik (3), except that the heterologous internal control (β -actin) and each virus were detected separately. Briefly, the 3 RT-qPCRs were performed with the AgPath-ID One-Step RT-PCR kit (Applied Biosystems) by using a total volume of 25 μL . Primer and probes used in this study are listed in the Technical Appendix 1 Table). A master mix consisting of 4.5 μL RNase-free water, 12.5 μL $2 \times$ RT-PCR buffer, 1.0 μL $25 \times$ RT-PCR enzyme mix, 2.0 μL SBV-specific (BVDV- or β -actin-specific) primer-probe mix (10 μM target-specific primers + 1.875 μM target-specific probe) for 1 reaction, and 5 μL RNA template was added. For amplification of SBV RNA, the following temperature profile was used: 10 min at 45°C (RT), 10 min at 95°C (inactivation of RT and activation of Taq polymerase), followed by 42 cycles of 15 s at 95°C (denaturation), 20 s at 56°C (annealing), and 30 s at 72°C (elongation). For amplification of BVDV RNA, the temperature profile was the following: 10 min at 50°C , 2 min at 95°C , and 40 cycles of 15 s at 95°C (denaturation) and 30 s at 60°C (combined annealing and elongation). The detection of the bluetongue virus genome was performed according to Toussaint et al. (4) with slight modifications. Briefly, a pan-BTV 2-step RT-qPCR targeting genome segment-5 of bluetongue viruses was carried out, again with β -actin mRNA as internal control. The Gene Expression Master Mix (Applied Biosystems) was used for a first qPCR with the following conditions: 10 min at 95°C , then 45 cycles of 15 s at 95°C (denaturation) and 1 min at 58°C (combined annealing and elongation). The cutoff was set at 43 as determined by dilutions of the synthetic RNA controls according to Toussaint et al. (4). Positive and doubtful samples are then theoretically submitted to a segment-1 or a segment-7-specific

PCR as described in Garigliany et al. (5). Because the step-1 qPCR did not detect any positive or doubtful samples from the tissues examined here, the step 2 was not necessary. For the detection of the genetic material of the 3 viruses targeted, all reactions were carried out twice. In 90% of cases, the results were identical. Whenever the results were conflicting, a third RT-qPCR was performed, and the majority result was taken as definitive. A negative extraction control, and both a negative and a positive RT and amplification controls, were always included.

Refuting Idiopathic Arthrogryposis

The cause of the congenital arthrogryposis syndrome affecting the local Belgian Blue cattle population was recently assigned to a focal transversion in the splice acceptor region of the phosphatidylinositol glycan anchor biosynthesis class H (PIGH) intron 1. All animals were genotyped to exclude the possibility that this mutation contributed to the observed lesions using the 5' exonuclease diagnostic assay recently made available (Sartelet A et al., unpub. data).

References

1. Garigliany MM, Bayrou C, Kleijnen D, Cassart D, Desmecht D. Schmallenberg virus in domestic cattle, Belgium, 2012. *Emerg Infect Dis.* 2012;18:1512–4. [PubMed](http://dx.doi.org/10.3201/eid1809.120716)
<http://dx.doi.org/10.3201/eid1809.120716>
2. Bilk S, Schulze C, Fischer M, Beer M, Hlinak A, Hoffmann B. Organ distribution of Schmallenberg virus RNA in malformed newborns. *Vet Microbiol.* 2012;159:236–8. [PubMed](http://dx.doi.org/10.1016/j.vetmic.2012.03.035)
<http://dx.doi.org/10.1016/j.vetmic.2012.03.035>
3. La Rocca SA, Sandvik T. A short target real-time RT-PCR assay for detection of pestiviruses infecting cattle. *J Virol Methods.* 2009;161:122–7. [PubMed](http://dx.doi.org/10.1016/j.jviromet.2009.06.005)
<http://dx.doi.org/10.1016/j.jviromet.2009.06.005>
4. Toussaint JF, Sailleau C, Breard E, Zientara S, De Clercq K. Bluetongue virus detection by two real-time RT-qPCRs targeting two different genomic segments. *J Virol Methods.* 2007;140:115–23. [PubMed](http://dx.doi.org/10.1016/j.jviromet.2006.11.007) <http://dx.doi.org/10.1016/j.jviromet.2006.11.007>
5. Garigliany M, De Leeuw I, Kleijnen D, Vandenbussche F, Callens J, Van Loo H, et al. The presence of bluetongue virus serotype 8 RNA in Belgian cattle since 2008. *Transbound Emerg Dis.* 2011;58:503–9. [PubMed](http://dx.doi.org/10.1111/j.1865-1682.2011.01230.x) <http://dx.doi.org/10.1111/j.1865-1682.2011.01230.x>

Technical Appendix Table. Primers and probes

Target	Primer/probe name	Sequence (5'→3')†	Genome position
SBV	382-F	TCA GAT TGT CAT GCC CCT TGC	382–402‡
	469-R	TTC GGC CCC AGG TGC AAA TC	450–469‡
	P-408	FAM-TTA AGG GAT GCA CCT GGG CCG ATG GT-BHQ1	408–433‡
BVDV	106-F	CCA TGC CCT TAG TAG GAC TAG C	106–127§
	190-R	GCG TCG AAC CAC TGA CGA CT	190–209§
	P-162	FAM-TGG ATG GCT TAA GCC CTG AGT ACA G-EDQ	162–186§
BTV	F_1–19	GGC AAC YAC CAA ACA TGG A	1–19¶
	R_76–57	AAA GTY CTC GTG GCA TTW GC	57–76¶
	P_49–27	FAM-CYC CAC TGA TRT TGT ATT TTC TCA A-TAMRA	49–27¶
β-actin	F_1005–1029	CAG CAC AAT GAA GAT CAA GAT CAT C	1005–1029
	R_1135–1114	CGG ACT CAT CGT ACT CCT GCT TT	1114–1135
	P_1081–1105	FAM-TCG CTG TCC ACC TTC CAG CAG ATG T-TAMRA	1081–1105

*SBV, Schmallenberg virus; BVDV, bovine viral diarrhea virus; BTV, bluetongue viruses; FAM = 6-carboxyfluorescein; EDQ, Eclipse Dark Quencher; BHQ1, Black Hole Quencher-1.

†Reverse primers complementary to positive-sense target strand.

‡In the SBV genome segment-S (GenBank accession no. HE649914).

§In the BVDV NADL genome (GenBank accession no. M31182)

¶In the BTV genome segment-5.

Natural Intrauterine Infection with Schmallenberg Virus in Malformed Newborn Calves

Technical Appendix 2

Gross Pathology and Histology

The Body as a Whole

Schmallenberg virus (SBV)-positive calves were significantly lighter than SBV-negative calves (32 ± 15 vs. 49 ± 4 kg, $p < 0.05$). The large deviation between SBV cases denotes a heterogeneous deficit of body weight. Notably, there was an obvious correlation between the body mass deficit and the severity of deformations in whole-body conformation (Table 1). Also, most deformed animals died spontaneously within 24 hours after birth (scores whole-body deformity score [WBD]-2 and -3). Among the least affected, the majority was euthanized. No significant morphologic changes were noted in the thoracic and abdominal cavities and organs.

The Axial Musculoskeletal System

Overall, permanent deviations of the axial skeleton in all 3 planes were observed (Technical Appendix 3 Figures 1, 2, <http://wwwnc.cdc.gov/EID/article/20/8/12-1890-Techapp3.pdf>). The most common observation (11/15) was a lateral deviation of the cervical spine (torticollis). In 2 cases (WBD-2), lateral deviations of the thoracic segment of the spine was noticed. In addition, in the most distorted animals (WBD-3), the torticollis was accompanied by a dorso-ventral deviation of the thoracolumbar spine (either kyphosis or lordosis) and by a gradual rotation of the column itself, giving it a helical conformation. In the most severe cases (WBD-3), the vertebrae displayed deformities, with distortions in the shape of the spinal canal but without stenosis. Besides, deficits in muscle mass in the spinal muscles were observed in all cases. Regarding their magnitude and distribution, no consistent pattern was identified. These changes seemed consistent with prenatal occurrence of processes leading to hypoplasia and/or atrophy. In addition, after section, muscles revealed whitish and multifocally distributed areas.

The Appendicular Musculoskeletal System

Most cases (13/15) displayed joint fixation of 1 or all joints of ≥ 1 limbs, which is referred to as arthrogryposis. Joint involvement was always symmetric (right/left ratio = 1), whereas tetramelic involvement was observed in the most severe cases only (WBD-3). When a single pair of limbs was involved, it almost always was the forelimbs. The joints were fixed either in hyperflexion (66% of affected joints) or in hyperextension. Section of the tendons always restored the mobility of the corresponding joint, and articular cavities were filled with a normal yellow viscous synovial fluid. Tendons spanning fixed joints were shorter than expected, and corresponding muscles displayed altered mass (decreased) and color (multifocal whitish patches). On visual inspection, bone lengths remained proportional to the size of the calves, but some articular surfaces deviated from the plane expected.

The Head

The general shape of the head was often altered, but the magnitude of the changes was not correlated with axial and appendicular musculoskeletal changes (Technical Appendix 3 Figure 3). Two calves displayed a horse-like (long nose and reduced height of cranial cavity) and 2 others a pig-like head (increased height and reduced length), 4 calves were brachygnathic (upper teeth protruding beyond lower teeth) and 1 prognathic (lower jaw too far forward). Notably, the head of a third of the calves displayed diverging sagittal axes, with an angle between the sagittal plane of the upper and lower halves of the head (Technical Appendix 3 Figure 3). There was no evidence of muscle injury or mandibular arthritis.

The Central Nervous System

Major alterations were systematically observed after the skull and spinal canal were opened (Figure 1; Technical Appendix 3 Figure 4). These changes involved the spinal cord and the telencephalon, whereas the brainstem (medulla oblongata, pons, mesencephalon, and diencephalon) and cerebellum were intact (except 1 hypoplastic cerebellum). In WBD-2 and -3 cases, a decrease in the cross-sectional area of the spinal cord was observed over its entire length (Technical Appendix 3 Figure 4). Because the width of the spinal canal remained similar to that of healthy calves, a large space filled with cerebrospinal fluid (CSF) was always interposed between the spinal cord and most of the canal circumference. In addition, the general structure of the spinal cord was preserved, with an intact ventral median fissure and a normally proportioned central canal. These changes are referred to as micromyelia without myelodysplasia and seem consistent with prenatal occurrence of processes leading to hypoplasia and/or atrophy. Remarkably, the magnitude of the decrease in spinal cord cross-

sectional area, as measured by the occipital ratio, correlated positively with the severity of axial and appendicular musculoskeletal deformities (Technical Appendix 3, Figure 5). Moreover, the neopallial part of the telencephalon was nearly completely absent in most SBV cases, whereas the paleopallium-olfactory components, the archipallium-hippocampus, fornix and basal nuclei were comparatively spared (Figure 1). The amount of CSF was consistently increased due to the filling of the space normally occupied by the neopallium. These macroscopic alterations produced 3 distinct morphotypes. In some calves, multiple, bilateral, and randomly located cystic cavities were detected in the neopallium, most of which communicated with the ipsilateral ventricle. These alterations were referred to as porencephaly. In other cases, all that remained from the neopallium was a thin, nearly transparent membrane with sometimes a few floating smooth-surfaced islets resembling cortex. The membrane was kept distended by the CSF that filled the space normally occupied by cerebral tissue. These changes were referred to as hydranencephaly. Finally, in a third subset of cases, the brain appeared normal after the skull was opened but revealed a severe, bilateral and symmetrical dilatation of lateral ventricles after section.

Histopathology

Brain

No significant alterations were seen in the brainstem and cerebellum (Technical Appendix 4 Table 2). In particular, the neuron number was not reduced; there was no perivascular cuffing of lymphocytes, no hemorrhages, no hemosiderin-laden macrophages, no mineralization, no gliosis, nor stigmata of periependymal inflammation. In the telencephalon, only minor changes were seen. In porencephalic cases, the cavities were lined by astrocytes and surrounded by occasional foci of gliosis. The membrane typical of hydranencephaly consisted mostly of astroglia, pia mater, blood vessels, and sometimes a few inflammatory cells. The thinned neopallium accompanying hydrocephaly was not remarkable either, again showing evenly distributed gliosis.

Spinal Cord

Examination of the spinal cord by light microscopy instantly revealed a very significant decrease in the neuron numbers along its entire length (Table 2). Conversely, like the encephalon, the presence of changes characteristic of recent or past necrosis or inflammation was not obvious. There was no perivascular cuffing of lymphocytes, no mineralization, no hemorrhages, no hemosiderin-laden macrophages. Some foci of gliosis and images consistent of neuronophagia were observed, but they remained very rare. In the most deformed animals

(WBD-3), there were no motor neuron left in the gray matter and no efferent axons in the ventral horns (Figure 2). Generally, the deficit in motor neurons was more pronounced than the deficit in sensory neurons (Table 2). Finally, there was an inverse correlation between the number of spinal neurons and the magnitude of whole-body deformation (Table 2).

Muscles

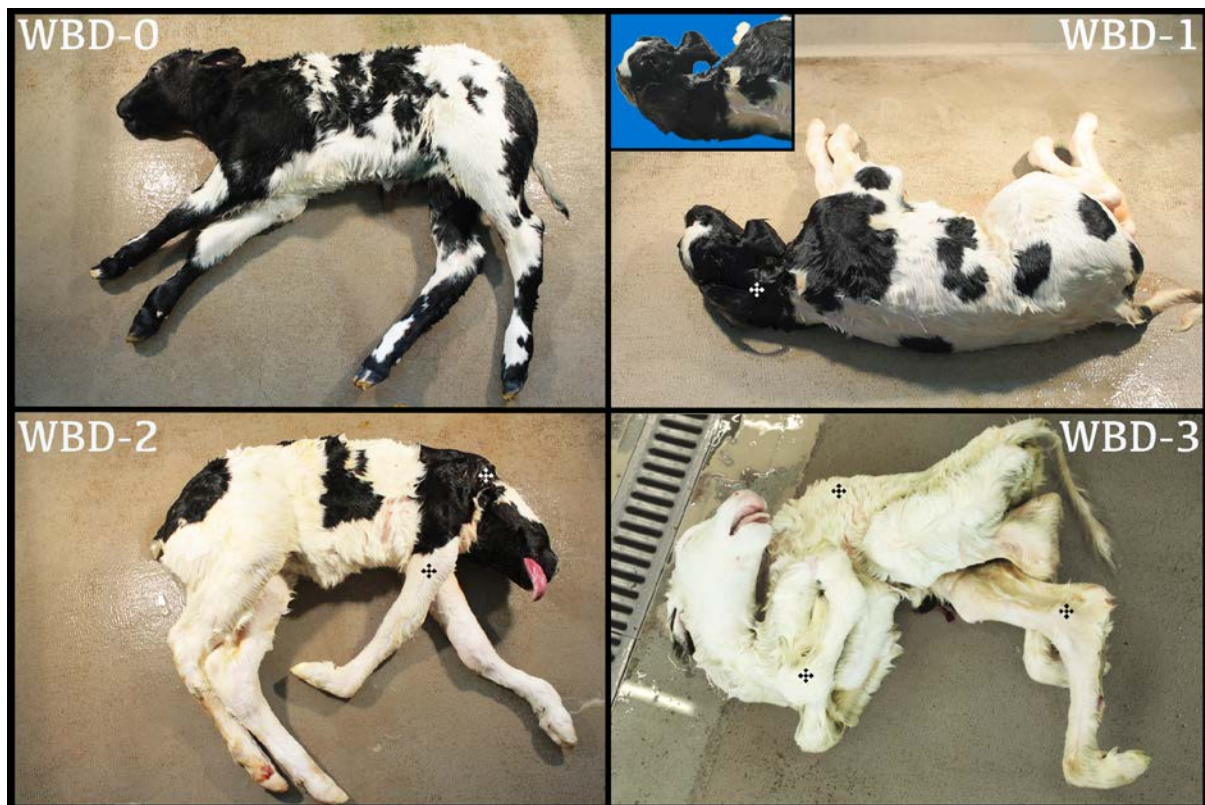
Apart in muscle parts injured by prolonged decubitus, changes characteristic of ongoing necrotizing or inflammatory processes were absent. In particular, hypercontraction bands, myofibers containing eosinophilic coagulum, leukocytic invasion and mineralization were absent. Conversely, muscle sections consistently displayed a diffuse pattern of increased fiber size variation with connective and adipose tissue infiltrations (Technical Appendix 3 Figure 6; Technical Appendix 4 Table 1). Large-diameter fibers were admixed with severely atrophied fibers, and islets of muscle-like tissue were dissected from each other by variable size areas where myofibers were replaced by fibrous connective and adipose tissues. In addition, myotubes were consistently observed in most-altered muscles examined, suggesting widespread attempts of regeneration and repair. Although the nature of the morphologic changes was the same throughout the muscles examined, their magnitude, as judged from the muscle/connective tissue ratio, varied from place to place which explains the scattered whitish plaques observed macroscopically.

Other Organs

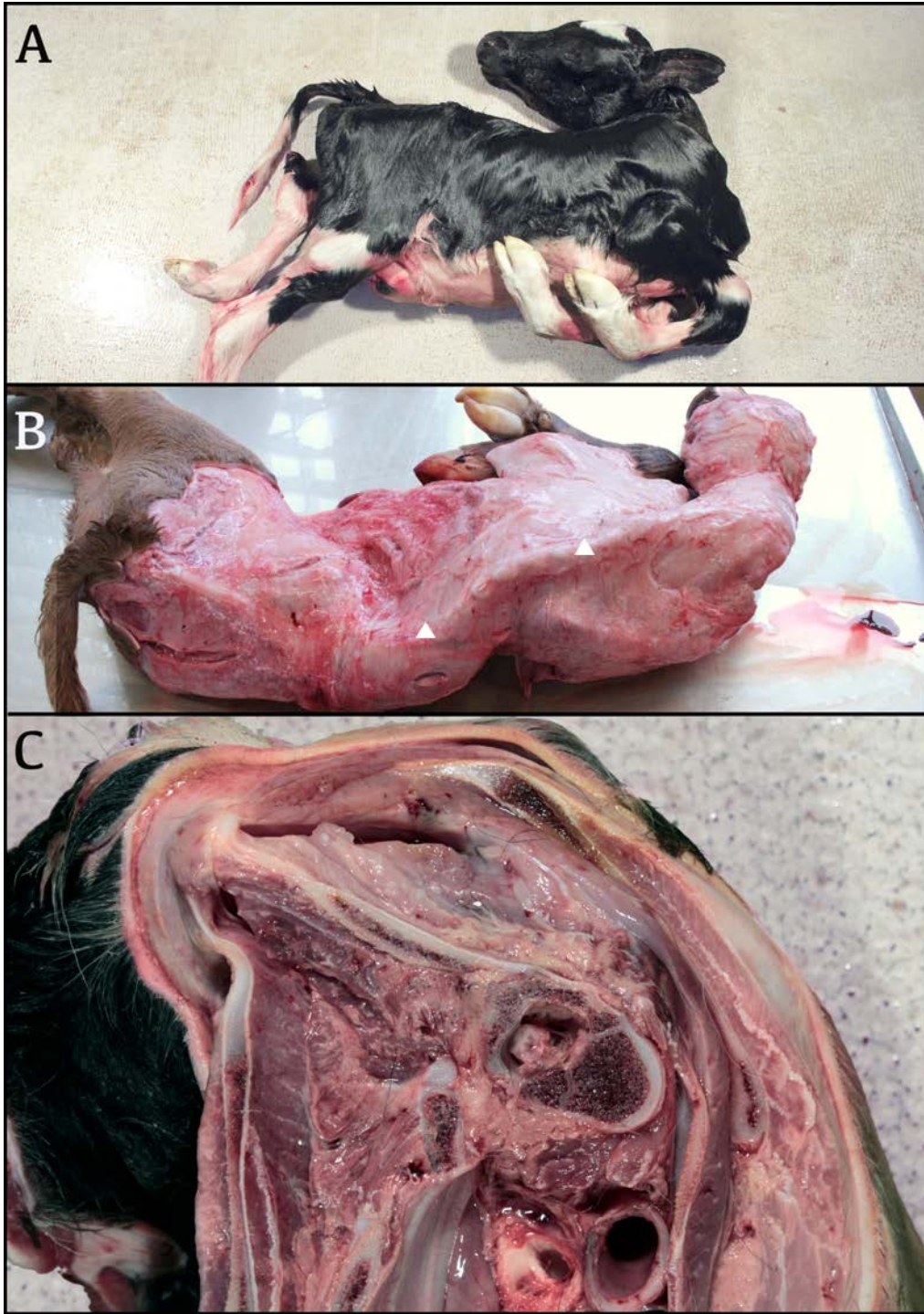
No reproducible lesion was observed in other thoracic or abdominal organs. A lymphocytic infiltration of the small intestine submucosa was noticed in the majority of SBV cases, hepatocytes swelling, increased granularity and eosinophilia in 6 cases and a lymphocytic interstitial pneumonia in 5 cases (Technical Appendix 4 Table 3).

Natural Intrauterine Infection with Schmallenberg Virus in Malformed Newborn Calves

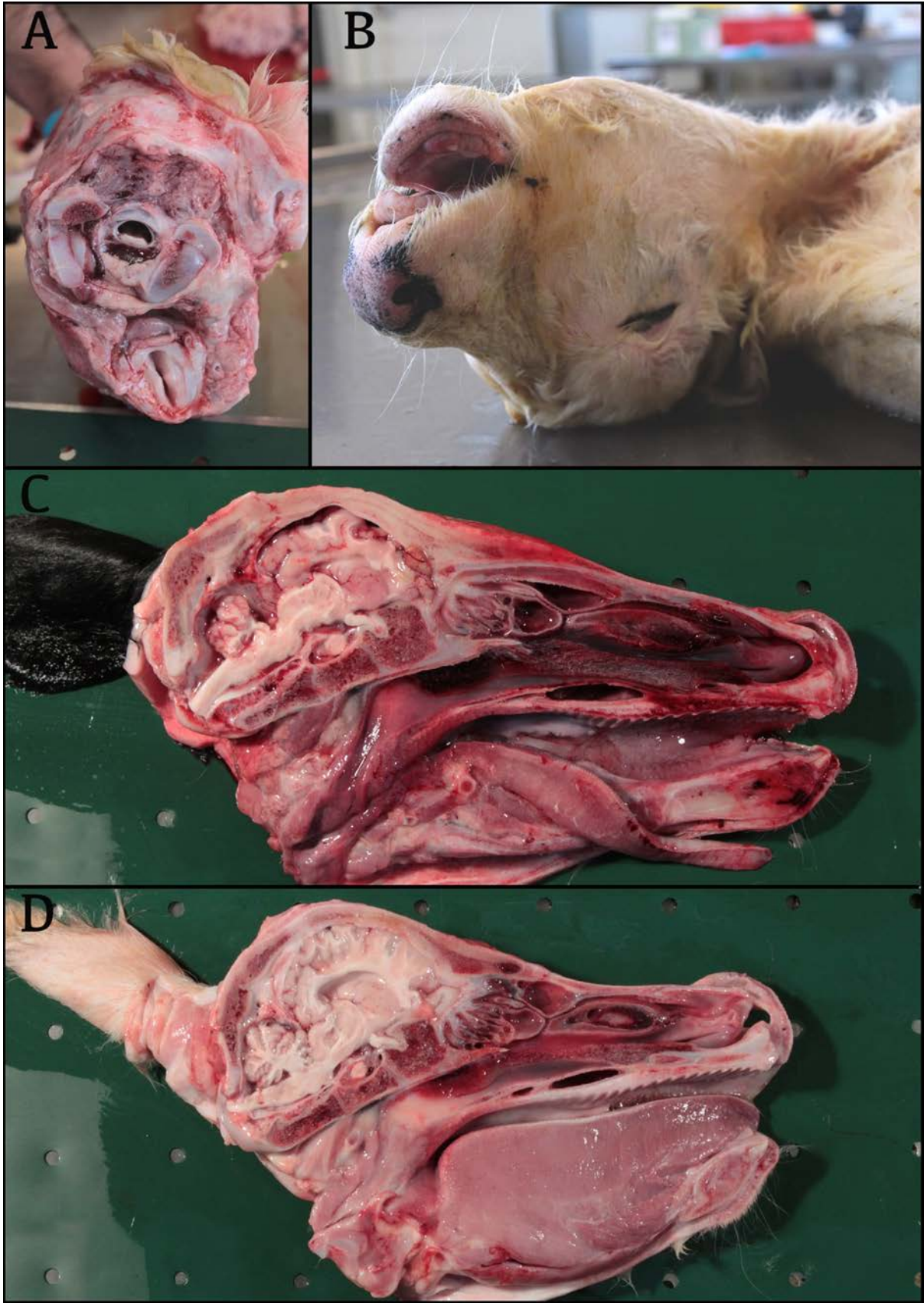
Technical Appendix 3



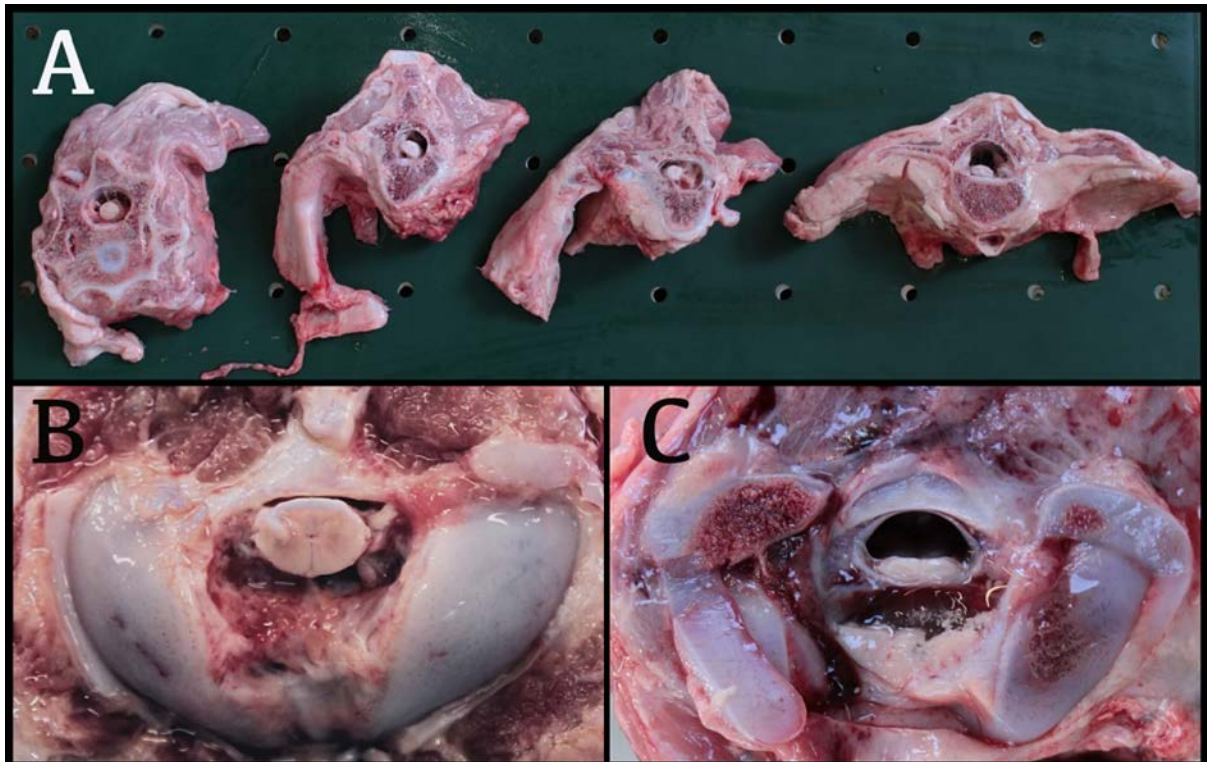
Technical Appendix Figure 1. Definition of whole-body deformity (WBD) scores in Schmallenberg virus (SBV)-infected newborn calves, Belgium, 2012. Animals with neurologic signs and apparently normal body shape were given a WBD score of 0. Those with altered body shape were scored 1, 2, or 3 depending on whether 1, 2 or 3 skeletal segments were deformed, respectively (spine, forelimbs, or hind limbs). Marks: deformed skeletal segments.



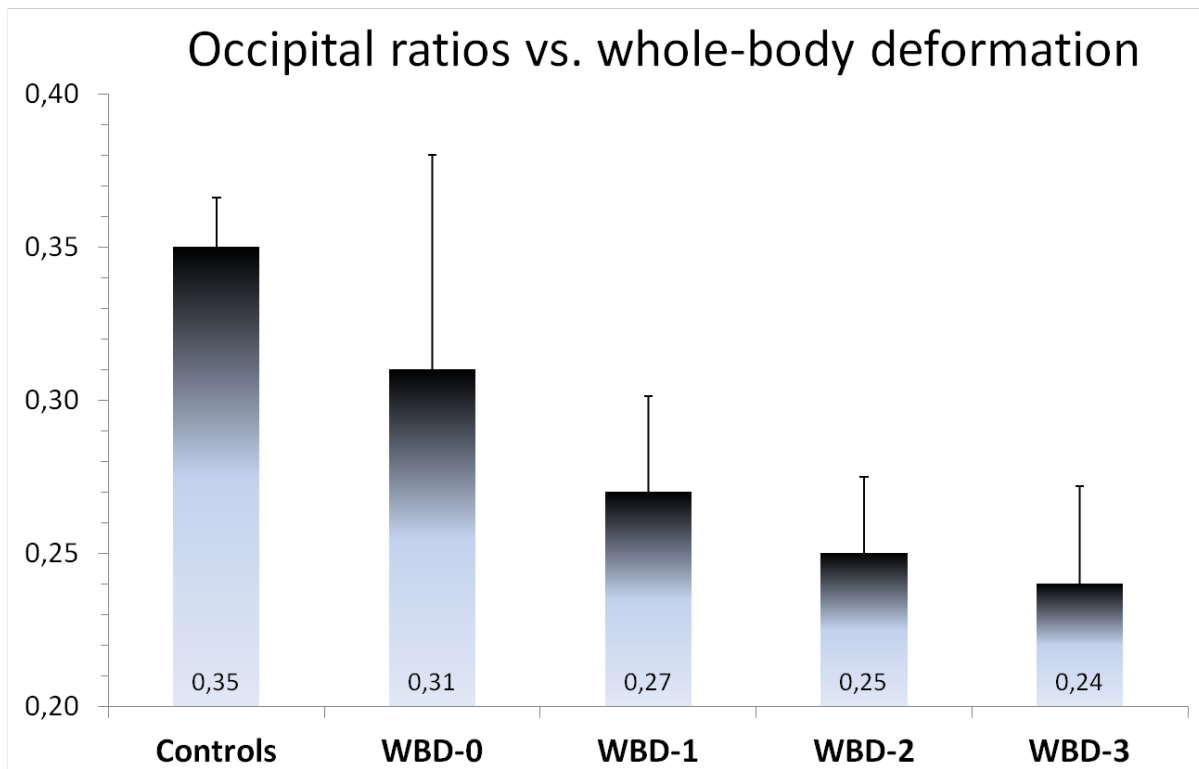
Technical Appendix Figure 2. Deformities of the axial skeleton in Schmallenberg virus–infected calves. A) Torticollis. B) Lateral deviations and asymmetric loss of musculus longissimus dorsi volume (compare left and right muscle mass at the triangles). C) Loss of volume and discoloration of right cervical muscles.



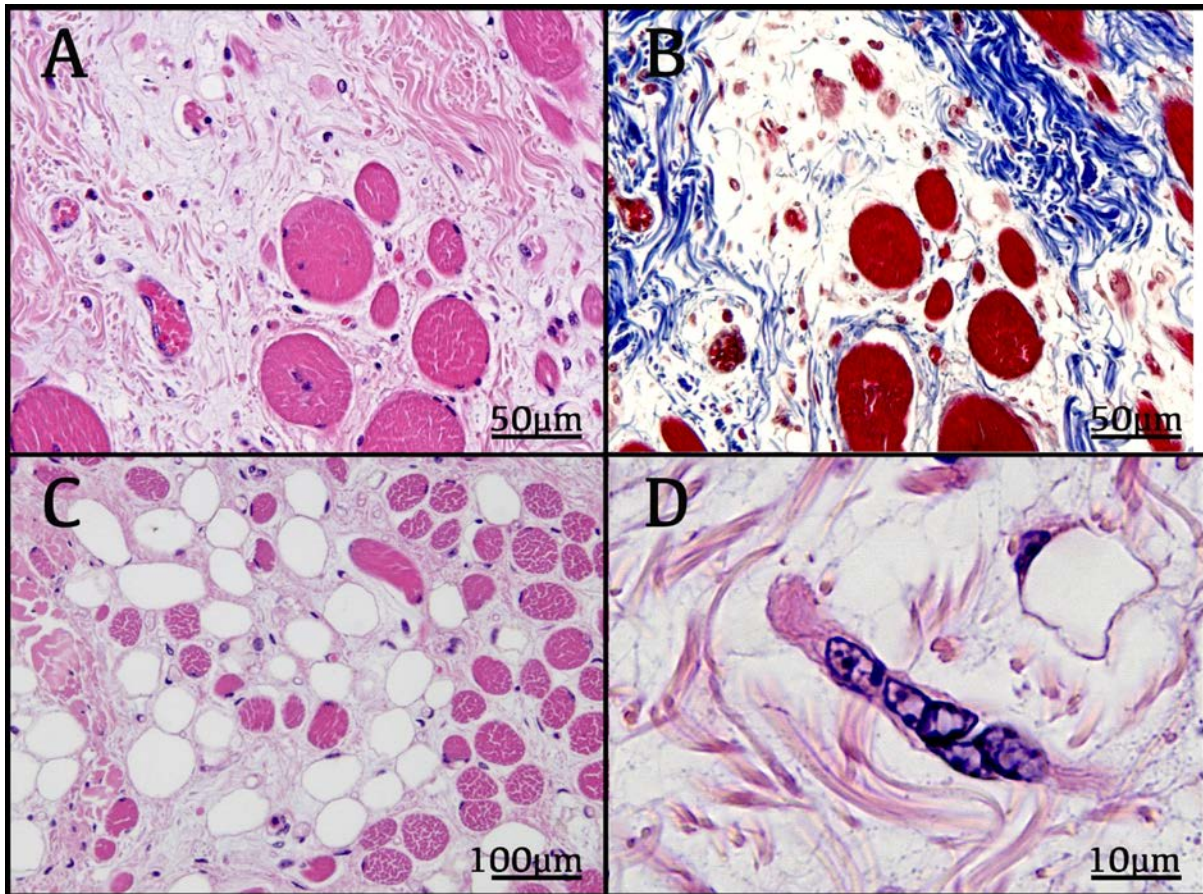
Technical Appendix Figure 3. Deformities of the head in Schmallenberg virus–infected calves. A) Diverging sagittal axes. B) Brachygnathism. Horse-like (C) and pig-like (D) profiles.



Technical Appendix 4. Micromyelia in Schmallenberg virus–infected calves. A) Successive sections showing micromyelia extending over the entire length of the spinal cord. B) Cross-section of spinal cord when it emerges from the foramen magnum in a control calf. C) The same in an SBV-positive calf.



Technical Appendix 5. Occipital ratios (mean \pm SD) in control and Schmallenberg virus-positive calves. Note negative correlation with whole-body deformity scores. The maximum width of the foramen magnum and of the spinal cord at that level were measured. The occipital ratio of a specific calf is the result of dividing the second width by the first.



Technical Appendix 6. End-stage muscles in a typical Schmallenberg virus–infected calf. Age- and site-matched histologic sections of semispinalis capitis muscle. A) Large-diameter fibers were admixed with severely atrophied fibers, and islets of muscle-like tissue were dissected from each other by variable size areas where myofibers were replaced by fibrous connective tissue (B) and by fat (C). D) A myotube suggesting an attempted regeneration. Hematoxylin and eosin (A, C, D) and Masson's trichrome (B) stains. Original magnification $\times 100$ (C), $\times 200$ (A, B), and $\times 1,000$ (D).

Natural Intrauterine Infection with Schmallenberg Virus in Malformed Newborn Calves

Technical Appendix 4

Technical Appendix Table 1. Distribution of microscopic lesions and virus-specific RNA in the skeletal muscles of 15 SBV-infected newborn calves*

Skeletal muscle	WBD/calf ID														
	WBD-0		WBD-1				WBD-2				WBD-3				
	A	B	C	D	E	F	G	H	I	J	K	L	M	N	O
Spinal muscles															
Musculus semispinalis capitis, cas															
RT-qPCR	NT		-	-	-	-	-	-	NT	-	-	-	-	-	-
Histology	NT	0	0	0	3	0	3	3	NT	3	3	3	3	3	3
Musculus semispinalis capitis, ces															
RT-qPCR	NT	-	-	-	-	-	-	-	NT	-	-	-	-	-	-
Histology	NT	1	0	0	2	0	3	3	NT	3	3	3	3	3	3
Musculus longissimus thoracis															
RT-qPCR	NT	-	-	-	-	-	-	-	NT	-	-	-	-	-	-
Histology	NT	0	0	0	0	0	0	0	NT	0	2	3	3	1	2
Forelimb muscles															
Musculus supraspinatus															
RT-qPCR	NT	-	-	-	+	-	-	-	NT	-	-	-	-	-	-
Histology	NT	0	0	0	0	0	0	0	NT	0	2	3	3	1	2
Musculus extensor carpi radialis															
RT-qPCR	NT	-	-	-	+	-	-	-	NT	-	-	-	-	-	-
Histology	NT	1	0	0	0	0	0	0	NT	1	3	3	3	0	3
Musculus flexor carpi ulnaris															
RT-qPCR	NT	-	-	-	+	-	-	-	NT	-	-	-	-	-	-
Histology	NT	1	0	0	1	0	0	0	NT	3	3	3	3	2	3
Hind limb muscles															
Musculus semimembranosus															
RT-qPCR	NT	-	-	-	+	-	-	-	NT	-	-	-	-	-	-
Histology	NT	0	1	0	0	0	0	3	NT	3	3	3	3	3	3
Musculus quadriceps femoris															
RT-qPCR	NT	-	-	-	+	-	-	-	NT	-	-	-	-	-	-
Histology	NT	0	0	0	1	0	3	3	NT	3	3	3	3	3	3
Musculus peroneus tertius															
RT-qPCR	NT	-	-	-	+	-	-	-	NT	-	-	-	-	-	-
Histology	NT	1	1	0	1	1	2	2	NT	0	3	3	3	3	3

*Extent of histologic changes was reported semiquantitatively by using a score of 0, 1, 2 or 3 depending on whether the histologically normal tissue extended over 100%, 75%–100%, 25%–75%, or <25% of the area examined and intensity of shading reflects this. SBV, Schmallenberg virus; WBD, whole-body deformity score; cas, concave side; RT-qPCR, reverse transcription quantitative PCR; NT, not tested; ces, convex side.

Technical Appendix Table 2. Distribution of microscopic lesions and virus-specific RNA in the CNS of 15 SBV-infected newborn calves

CNS portion	WBD/calf ID														
	WBD-0		WBD-1				WBD-2				WBD-3				
	A	B	C	D	E	F	G	H	I	J	K	L	M	N	O
Paleopallium															
RT-qPCR	NT	+	NT	-	+	+	-	-	NT	-	+	+	-	-	-
Histology	NT	GL	0	0	GL	GL	0	0	NT	0	0	0	0	0	0
Neopallium															
RT-qPCR	+	+	-	+	+	+	+	+	+	+	+	+	-	+	+
Histology	0	GL	0	G	GL	0	0	0	NT	GL	0	0	0	0	0
Diencephalon															
RT-qPCR	NT	+	NT	-	+	+	+	-	NT	-	+	+	-	+	-
Histology	NT	0	0	GL	GL	0	0	0	NT	0	GL	0	0	0	0
Mesencephalon															
RT-qPCR	NT	+	NT	-	+	+	+	+	NT	+	+	+	+	+	-
Histology	0	0	0	0	0	0	0	0	NT	0	GL	0	0	0	0
Cerebellum															
RT-qPCR	NT	+	NT	-	+	+	-	+	NT	-	-	+	-	-	-
Histology	0	0	0	ED	0	0	0	0	NT	0	0	0	0	0	0
Pons															
RT-qPCR	NT	+	NT	-	+	+	+	+	NT	-	+	+	-	+	-
Histology	0	0	0	ED	0	0	ED	0	NT	0	ED	0	0	0	0
Spinal cord†															
RT-qPCR	NT	+	+	+	+	+	+	+	+	+	+	+	-	+	+
Histology	NT	0	0	ED	0	0	0	ED	NT	ED	ED	ED	ED	0	ED

*CNS, central nervous system; SBV, Schmallenberg virus; WBD, whole-body deformity score; 0, no lesion; RT-qPCR, reverse transcription quantitative PCR; +, positive; -, negative; GL, gliosis; ED, edema; †Sections were made at the level of the fourth cervical vertebra.

Technical Appendix Table 3. Distribution of microscopic lesions and virus-specific RNA in thoraco-abdominal organs of 15 SBV-infected newborn calves*

Organ	WBD/calf ID														
	WBD-0		WBD-1				WBD-2				WBD-3				
	A	B	C	D	E	F	G	H	I	J	K	L	M	N	O
Thorax															
Lung															
RT-qPCR	-	-	-	+	+	+	+	-	-	-	-	-	-	+	-
Histology		IP		IP		IP			NT		NT			IP	
Thymus															
RT-qPCR	NT	-	-	-	-	-	-	-	-	-	-	-	-	-	-
Histology	NT								NT		NT				
Myocardium															
RT-qPCR	NT	-	-	-	+	-	-	-	-	-	-	-	-	-	-
Histology	NT								NT		NT				
Abdomen															
Duodenum															
RT-qPCR	NT	-	-	-	-	-	-	-	-	-	-	-	-	-	-
Histology	NT								NT		NT			HL	
Jejunum															
RT-qPCR	-	-	-	-	-	-	-	-	-	-	-	-	-	-	-
Histology	LI			HL					NT	LI	NT		HL	HL	HL
Ileum															
RT-qPCR	-	-	-	-	-	-	-	-	-	-	-	-	-	-	-
Histology	HL			HL	HL	HL	HL	HL	NT	HL	NT		HL	HL	HL
Colon	NT	-	-	+	-	+	-	-	-	-	-	-	-	-	-
RT-qPCR															
Histology	NT								NT		NT				
Kidney															
RT-qPCR	-	-	-	-	+	-	-	-	-	-	-	-	-	-	-
Histology									NT		NT				
Liver															
RT-qPCR	-	-	-	-	+	-	-	-	-	-	-	-	-	-	-
Histology		DEG		DEG		DEG		DEG	NT		NT	DEG	CON	DEG	
Spleen															
RT-qPCR	-	-	-	-	+	-	-	-	-	-	-	-	-	-	-
Histology									NT		NT		CON		

SBV, Schmallenberg virus; WBD, whole-body deformity score; RT-qPCR, reverse transcription quantitative PCR; NT, not tested; +, positive; -, negative. Histologic alterations are as follows: CON, congestion; DEG, degeneration; LI, leukocytic infiltration; IP, interstitial pneumonia. HL, lymphoid hyperplasia. Blank spaces denotes absence of alteration.

Natural Intrauterine Infection with Schmallenberg Virus in Malformed Newborn Calves

Technical Appendix 5

Diagnostic Considerations

Virus Detection

To our knowledge, there is currently 1 well-documented source with which to compare the rate of detection of Schmallenberg virus (SBV) RNA in suspected SBV cases (*1*). At first sight, these detection rates appear very different. This is, however, not surprising because the definition of a suspected SBV case is very different between the 2 studies. For De Regge et al., a suspected case was an aborted calf with the typical malformations described for SBV infection: arthrogryposis, hydranencephaly, or hypoplasia of cerebrum and/or cerebellum (*1*). With this definition, 38% of the suspected cases proved SBV RNA positive. In the present study, we considered that, in spring 2012, the whole spectrum of SBV-related conditions in the bovine species was, by definition for a disease that had emerged 2 months before, unknown. This is the reason we opted for a broader definition of suspected SBV cases: 1) calves with neurologic signs after death or 2) calves with musculoskeletal deformities or 3) calves in which no unequivocal cause of death was identified at necropsy. By using this broader definition, 22% of suspected cases proved SBV RNA positive. Further, if we restrict the cohort of suspected SBV cases to those compatible with the afore-described narrow definition, we then had 15 suspected cases in total, of which 13 proved SBV RNA positive, thus a detection rate of 87%. In this instance, the starting cohort is similar, except that aborted calves were tested on the one hand (*1*), and calves born at term on the other (this study). Considering the methodologic aspects, it seems that the higher rates we observed could be due to 1 difference or to the combination of 3 differences, each with increasing sensitivity. First, we stored the tissue samples at -80°C often within 24 h after death and, in all cases, within 48 h, which is favorable to conserving viral RNA. Second, the extraction procedure implemented in this study (TRIzol) is deemed more efficient than using commercially available kits. Third, whereas SBV and β -actin RNAs were amplified together in a duplex

assay in the first study (1), we amplified SBV RNA and β -actin RNA separately, which, in our hands, results in a higher sensitivity than do duplex assays.

To our knowledge, this study is the most comprehensive so far in terms of distribution of SBV RNA in the calf naturally infected in utero (26 sites were tested, cf. Technical Appendix 4 Tables 1–3). It clearly appears that testing the spinal cord at C4 maximizes the probability of detecting the virus (93%). The viral RNA is also often present in the neopallium (87%) and the mesencephalon (83%). Taking a fragment at each of these 3 sites and pooling them for reverse transcription quantitative PCR can detect all, which confirms recently published reports (1,2). For cons, the paleopallium, diencephalon, and cerebellum seem definitely not suitable for diagnosis. Furthermore, we show that the lymphoid and related organs (spleen, thymus, liver) contain the virus only very rarely (1 of 15 calves), which suggests that SBV is not lymphotropic. Finally, the screening of the organs revealed that the virus is quite frequently detectable in the lungs (one third of cases). This result is surprising because, unlike the CNS, lungs are exposed to circulating antibodies. This observation may reflect an important aspect of the biology of the new virus in its ruminant host.

Field Diagnosis

The data suggest that, in the field and when resources are limited, relying on precolostral positive serology to assign the cause of a congenital triad por-/hydranencephaly-micromyelia-arthrogryposis to SBV is rarely wrong. This conclusion is obviously valid only in areas where phylogenetically related viruses, those likely to cause cross-reactions, are absent. In the present context, the cause of all cases of arthrogryposis undergoing necropsy during January 1–June 30, 2012, was established: either the SBV genetic material or SBV IgGs were detected, or the animal was homozygous for the *PIGH* mutation. The presence of this genetic defect in a population does not, however, hamper the differential diagnosis in field situations: the genetically determined arthrogryposis syndrome does not include por-/hydranencephaly or micromyelia. Further, the calves concerned always displayed a cleft palate, which was never observed among SBV cases.

References

1. De Regge N, van den Berg T, Georges L, Cay B. Diagnosis of Schmallenberg virus infection in malformed lambs and calves and first indications for virus clearance in the fetus. *Vet Microbiol.* 2013;162:595–600. [PubMed http://dx.doi.org/10.1016/j.vetmic.2012.11.029](http://dx.doi.org/10.1016/j.vetmic.2012.11.029)

2. Bilk S, Schulze C, Fischer M, Beer M, Hlinak A, Hoffmann B. Organ distribution of Schmallerberg virus RNA in malformed newborns. *Vet Microbiol.* 2012;159:236–8. [PubMed](#)
<http://dx.doi.org/10.1016/j.vetmic.2012.03.035>

Natural Intrauterine Infection with Schmallenberg Virus in Malformed Newborn Calves

Technical Appendix 6

Mechanistic Hypotheses Underlying Central Nervous System and Muscle Changes

Central Nervous System

From a mechanistic point of view, por- and hydranencephaly could result from destruction of the paraventricular germinal zone of the telencephalon, as well as of the neocortex that is already formed. The mechanisms involved can broadly be separated into 2 types that are not mutually exclusive: 1) direct cytopathogenicity of SBV on neuronal and glial cells and 2) ischemic necrosis. In the present Schmallenberg virus (SBV)-positive cases, there was very little evidence for ischemic destruction. In particular, neither thrombosis or perivascular edema, nor sequelae of hemorrhages (erythrophagocytosis or hemosiderin-laden macrophages) were seen, which sharply contrasts with histologic reports describing the similarly cavitated brains of bluetongue virus-infected bovine fetuses (1). Conversely, our histologic findings resemble those characterizing the cavitated telencephalon of lambs infected by Cache Valley virus in utero (2). Selective nerve cell necrosis and subsequent cavitation were, therefore, supposed to result from the direct cytolytic action of the virus itself. Necrosis of paraventricular immature, rapidly dividing neurons would prevent the outward migration of neuroblasts and subsequent maturation of the cerebral cortex and cause hypoplasia, whereas necrosis of established neocortical neurons would result in atrophy. In both cases, cavitation of necrotic areas then follows, the distinction between hydranencephaly and porencephaly being a matter of degree. A third subset of calves showed symmetrical dilatation of the lateral ventricles with corresponding thinning of the cortex (hydrocephaly). Logically, one of the causes of such damage is a stenosis of the mesencephalic aqueduct (3,4). When this happens, the lateral ventricles expand primarily at the expense of the neopallium (necrosis by compression) because the resistance of the diencephalon to mechanical constraints seems higher. The stenosis may result either from a developmental

disorder associated with a genetic defect (5) or from a prenatal or postnatal periependymal inflammation. It is tempting to invoke the latter mechanism here because a post-inflammatory stenosis of the aqueduct with secondary hydrocephaly has already been demonstrated in kittens and puppies infected in utero by the feline parvovirus (3) or canine parainfluenza virus, respectively (4). Unfortunately, we have not been able to confirm the existence of significant tissue remodeling around the aqueduct, which leaves the question of the origin of hydrocephaly unresolved. The systematic lack of signs of inflammation in the telencephalons yet highly deformed and in which the genetic material of the virus is still present is a remarkable feature of the cohort examined here. This absence suggests that infection occurred early during gestation, when the host response to infection is still limited and subsides to inapparent microscopic changes at term (6,7). Regarding the cerebellum, the observations gathered here (hypoplasia in a single calf) contrast with those reported recently by which about 40% of calves infected in utero displayed a cerebellar hypoplasia at necropsy (8). This difference remains unexplained.

The degree of overall body deformity was correlated with a progressively greater reduction in the size of the spinal cord (as determined by spinal cord:foramen magnum ratio) and with reduced numbers of spinal neurons, suggesting that the lack of movement leading to arthrogryposis is a direct consequence of the spinal cord lesions leading to denervation atrophy of skeletal muscle. This primary role for the spinal cord lesion is further supported by the tendency of forelimbs and hind limbs to be affected bilaterally because muscle involvement might be expected to lead to more randomly distributed lesions.

Skeletal Muscles

Taken together, the macroscopic and microscopic changes in skeletal muscles are compatible with several distinct lesions: 1) atrophy, 2) compensatory hypertrophy, 3) chronic polymyositis, 4) lipomatosis, and 5) attempts to regenerate. The coexistence of these lesions is characteristic of so-called end-stage muscles, i.e., muscles in which processes are long at work. This picture is consistent with denervation atrophy as aforesaid, but a virus-induced necrotizing polymyositis could have contributed as well. In this respect, the detection of SBV genetic material in all skeletal muscles of animal E suggests that the fetal muscles are permissive to the virus that could cause necrosis by a direct cytolytic effect on myofibers as Akabane and Cache Valley viruses do (3,9). In addition, the question of why the virus was detected in the skeletal muscles of a single SBV-infected calf and never in the muscles of the other 14 remains unresolved.

References

1. MacLachlan NJ, Osburn BI. Bluetongue virus–induced hydranencephaly in cattle. *Vet Pathol.* 1983;20:563–73. [PubMed http://dx.doi.org/10.1177/030098588302000508](http://dx.doi.org/10.1177/030098588302000508)
2. Rodrigues Hoffmann A, Welsh CJ, Wilcox Varner P, de la Concha-Bermejillo A, Marchand Ball J, Ambrus A, et al. Identification of the target cells and sequence of infection during experimental infection of ovine fetuses with Cache Valley virus. *J Virol.* 2012;86:4793–800. [PubMed http://dx.doi.org/10.1128/JVI.06858-11](http://dx.doi.org/10.1128/JVI.06858-11)
3. Csiza CK, Scott FW, de Lahunta A. Feline viruses: XIV, transplacental infections in spontaneous panleukopenia of cats. *Cornell Vet.* 1971;61:423–39. [PubMed http://dx.doi.org/10.1177/030098588201900111](http://dx.doi.org/10.1177/030098588201900111)
4. Baumgärtner WK, Krakowka S, Koestner A, Evermann J. Acute encephalitis and hydrocephalus in dogs caused by canine parainfluenza virus. *Vet Pathol.* 1982;19:79–92. [PubMed http://dx.doi.org/10.1177/030098588201900111](http://dx.doi.org/10.1177/030098588201900111)
5. Cho DY, Leipold HW. Congenital defects in the bovine central nervous system. *Vet Bull.* 1977;47:489–504.
6. Barlow RM. Morphogenesis of hydranencephaly and other intracranial malformations in progeny of pregnant ewes infected with pestiviruses. *J Comp Pathol.* 1980;90:87–98. [PubMed http://dx.doi.org/10.1016/0021-9975\(80\)90031-6](http://dx.doi.org/10.1016/0021-9975(80)90031-6)
7. Huxtable C, Jubb KVF. The nervous system. In Jubb KVF, Kennedy PC, Palmer NC, editors. *Pathology of domestic animals.* Vol 1. 4th ed. San Diego (CA): Academic Press; 1993. pp 198, 270–86.
8. Herder V, Wohlsein P, Peters M, Hansmann F, Baumgärtner W. Salient lesions in domestic ruminants infected with the emerging so-called Schmallenberg virus in Germany. *Vet Pathol.* 2012;49:588–91. [PubMed http://dx.doi.org/10.1177/0300985812447831](http://dx.doi.org/10.1177/0300985812447831)
9. Konno S, Nakagawa M. Akabane disease in cattle: congenital abnormalities caused by viral infection. *Experimental disease. Vet Pathol.* 1982;19:267–79. [PubMed http://dx.doi.org/10.1177/030098588201900305](http://dx.doi.org/10.1177/030098588201900305)